Single-phase Grid-connected PV System with Golden Section Search-based MPPT Algorithm*

Shuang Xu[1*], *Riming Shao*[2], *Bo Cao*[3*] *and Liuchen Chang*[3]

(1. School of Electrical and Control Engineering, North China University of Technology, Beijing 100144, China;
2. R&D Department, Alpha Technologies Inc., Bellingham 98226, USA;
3. Emera and NB Power Research Centre for Smart Grid Technologies, University of New Brunswick, Fredericton E3B5A3, Canada)

Abstract: Maximum power point tracking (MPPT) is a technique employed for with variable-power sources, such as solar, wind, and ocean, to maximize energy extraction under all conditions. The commonly used perturb and observe (P&O) and incremental conductance (INC) methods have advantages such as ease of implementation, but they also have the challenge of selecting the most optimized perturbation step or increment size while considering the trade-off between convergence time and oscillation. To address these issues, an MPPT solution for grid-connected photovoltaic (PV) systems is proposed that combines the golden section search (GSS), P&O, and INC methods to simultaneously achieve faster convergence and smaller oscillation, converging to the MPP by repeatedly narrowing the width of the interval at the rate of the golden ratio. The proposed MPPT technique was applied to a PV system consisting of a PV array, boost chopper, and inverter. Simulation and experimental results verify the feasibility and effectiveness of the proposed MPPT technique, by which the system is able to locate the MPP in 36 ms and regain a drifting MPP in approximately 30 ms under transient performance. The overall MPPT efficiency is 98.99%.

Keywords: Grid-connected system, maximum power point tracking (MPPT), photovoltaic (PV) system, single-phase inverter

1 Introduction

The U.S. Energy Information Administration (EIA) estimates that photovoltaic (PV) generation increased from approximately 5 million kW • h in 1984 to approximately 107 billion kW • h in 2019 [1]. In a grid-connected PV system, a dc-ac inverter is modulated by pulse-width modulation (PWM) to convert the PV-generated dc power into grid-side ac power. The efficiency of power generation of a PV array is optimized by maximum power point tracking (MPPT) technology [2]. In a single-phase inverter system, the grid-side power pulsates at twice the grid frequency due to the multiplication of grid voltage and current, which causes suboptimal power generation from the PV array [3]. Therefore, an additional dc-dc converter is usually added to regulate the voltage and control the power drawn from the PV array [4].

Due to the nonlinear current-voltage (*I-V*) characteristics, there is a unique maximum power point (MPP) at a given irradiance and temperature in a PV system [5]. Significant work has been conducted on MPPT with grid-connected and standalone PV systems to maximize power extraction under all conditions [6-7], among which the perturb and observe (P&O), or hill-climbing method, is most widely used [8-9]. In the P&O method, the controller periodically adjusts the voltage or duty cycle by a small amount from the PV system and measures the power. If the power increases, further adjustments are made in that direction until the power no longer increases, and vice versa. This method is easy to implement, but at steady state, the operating point still oscillates around the MPP, which causes energy wastage. Moreover, it is difficult to select a proper perturbation step considering the trade-off between convergence time and oscillation [8]. Under some rapidly changing atmospheric conditions, it is well known that the P&O algorithm can face difficulty during such time intervals [10].

Regarding these problems with P&O, the incremental conductance (INC) algorithm was

Manuscript received July 16, 2021; revised October 15, 2021; accepted December 5, 2021. Date of publication December 31, 2021; date of current version December 16, 2021.
* Corresponding Author, E-mail: sxu1@unb.ca and E-mail: b.cao@unb.ca
* Supported in part by the Natural Sciences and Engineering Research Council of Canada, and in part by the Atlantic Innovation Fund.
Digital Object Identifier: 10.23919/CJEE.2021.000035

introduced in Ref. [11]. In the INC method, the controller tracks the MPP by comparing the derivative of the array power with respect to the array voltage. If the derivative is equal to zero, the power point is at the MPP; otherwise, it is at the left side of the MPP when the derivative is positive and at the right side when the derivative is negative. Hence, the INC algorithm is superior to P&O when determining the best direction of perturbation and identifying whether the MPP has been reached [10-12]. However, similar to P&O, there is a tradeoff between convergence time and oscillation when choosing the increment (step) size. As such, P&O and INC strategies with variable step size were proposed in Refs. [9, 13-14]. Regarding tracking accuracy and rate, MPPT algorithms with variable step size show better performance than those with fixed step size. However, they require deliberate tuning for parameter optimization because the increment or step is not a fixed value. These parameters are dependent on system characteristics. Instructions and principles for tuning the optimal values are provided in Refs. [8, 15].

Other MPPT techniques exist, such as the ripple correlation control method, which observes the phase commutation between the current and PV power to track the MPP quickly; however, it is difficult to measure the incremental PV power and phase commutation [7]. Some modern control strategies, such as fuzzy logic control and neural networks, have also been widely adopted as alternatives to P&O and INC due to their inherent nature of dealing with non-linear control objectives [16-17]. However, the effectiveness of fuzzy control strategies greatly depends on expertise in choosing the correct error computation. Similarly, neural network-based MPPT performance greatly depends on the design of the neuron layers and training weights, which limits its versality and flexibility. There are also some wind turbine and thermophotovoltaic system-specific MPPT algorithms [18-19]. Some comparisons have also been made among different MPPT techniques [20-23], but there is no de facto superior MPPT approach.

Nowadays, the partial shading condition is a critical issue in PV systems, especially in large-scale centralized PV systems, where the shaded PV modules must absorb power from non-shaded PV modules. There are multiple ways to deal with this problem. First, micro-inverters have been developed to be installed in each PV module, giving each PV module its own MPPT that does not affect the global MPPT of the entire PV array. Second, a bypass diode is connected in parallel with each PV module to provide an alternative path during partial shading [24], and in this manner, MPPT techniques considering the partial shading condition have been proposed, including the memetic salp swarm algorithm (MSSA) and dynamic leader collective intelligence (DLCI) method. Under high penetration of distributed energy resources (DERs), the risk of grid instability increases due to the intermittent and stochastic nature of renewable energy, and modern grid codes have been updated to include more renewable-related rules for DER inverters to provide power system support functions, such as voltage and frequency regulations. To include frequency regulation capability, DERs usually have pre-curtailment for active power reserve or headroom in the case of frequency contingency. Various power curtailment methods have been discussed in Refs. [25-26], shifting the operating point to the left or right side of the MPPT curves so that the DERs are operated at a lower power instead of the maximum power, but such methods are outside the scope of this study.

Regarding the drawbacks of the P&O and INC algorithms and the complexity of existing intelligent control algorithms, this paper proposes a multi-stage MPPT algorithm that includes a golden section search (GSS) method as a straightforward optimization approach targeting small-scale PV systems. In this method, an initial interval is first selected in the PV voltage range, which brackets the MPP. Then, the GSS method begins narrowing the width of the interval at the rate of the golden section number (φ=0.618) [27-28]. Therefore, the method will converge to the MPP with a shrinking rate of 0.618 for each round. As for locating the initial interval where the MPP search starts, the P&O method is applied to locate the vicinity of the MPP as the initial interval for GSS, and the perturbation used in P&O can be set as relatively large to speed up the search. As a result, the proposed multi-stage MPPT involves P&O in the first stage and GSS in the second stage, and the INC technique is used to verify the located MPP in the third stage, as

the system must know if the MPP has drifted when the conditions change. Therefore, the proposed multi-stage MPPT technique does necessitate a compromise between the convergence time and oscillation (as P&O and INC do) while maintaining the advantages of P&O and INC, such as ease of implementation and little search information requirement compared with other complicated algorithms.

The operating principle of the proposed GSS-based MPPT algorithm is described in Section 2. The system configuration and modeling of the single-phase grid-connected PV system with MPPT are described in Section 3. Simulation and experimental results that validate the GSS-based MPPT algorithm are presented and discussed in Section 4. Finally, the contributions of this study are summarized in Section 5.

2 GSS-based MPPT algorithm

The PV system topology, which consists of a PV array, boost chopper, dc-link capacitor, and single-phase grid-connected inverter, is illustrated in Fig. 1. The boost chopper and inverter are connected in series through the dc-link capacitor.

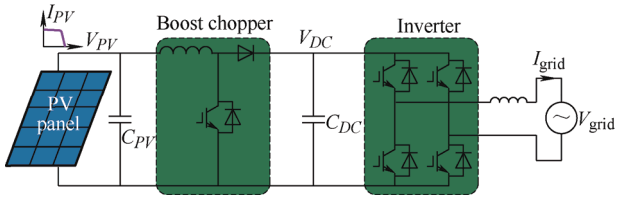

Fig. 1 Circuit of single-phase grid-connected PV system

The MPPT mechanism is integrated with the boost chopper. By decoupling the PV array from the inverter, it can extract maximum power from the PV array by regulating the proper PV output. Because the power injected into the grid by the single-phase inverter pulsates at twice the grid frequency, while a constant dc power is desirable at the PV output, a large electrolytic capacitor is paralleled at the dc-link to absorb the power imbalance. The instantaneous dc-link voltage also pulsates at twice the grid frequency because of the second-order power imbalance, but the average value of the dc-link voltage stays constant.

In this case, the balanced power flow control strategy for the inverter can be as simple as using an averaged dc-link voltage control. Then, the inverter uses only the dc-link voltage as a control variable and requires nothing from the boost chopper for its operation. The boost chopper and inverter are thus mutually independent, and the corresponding control is greatly simplified.

2.1 GSS method

The GSS method is used for locating the maximum or minimum of a strictly unimodal function inside a range by repeatedly narrowing the width of the range. For a unimodal function, as shown in Fig. 2, it is recognized that $f(x_3)>f(x_4)$ once the maximum value of the unimodal function lies on the left-hand side of x_3, as indicated by the dashed line, and $f(x_3)<f(x_4)$ once the maximum value lies on the right-hand side of x_4, as indicated by the straight line, and vice versa. As such, the maximum point is located within one of the two reduced intervals (x_1, x_4) and (x_3, x_2) after comparison between $f(x_4)$ and $f(x_3)$. Then, a new point subdivides the interval into two parts, and the wider range is used as the new search interval for the next iteration. When the number of iterations reaches the limit or the range shrinks to a certain value, the point inserted most recently can be considered as the maximum point [28].

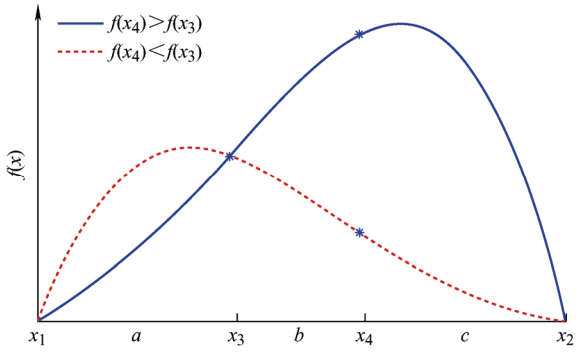

Fig. 2 GSS scheme for locating the MPP

As shown in Fig. 2, the main objective is to locate the maximum functional value within the range of (x_1, x_2). In each iteration, two points are selected such that each point subdivides the range into two parts that meet the golden section, which means the potential search section (x_3, x_2) or (x_1, x_4) in the next iteration has a width of 0.618× that in the previous iteration. The widths of the potential sections must be equal because the search speed will rapidly decrease if wider sections are chosen more frequently in some cases. Therefore, the inserted point x_4 must satisfy the

following equation

$$a=c \tag{1}$$

In this manner, the sections have the same proportion of spacing between the three points such that the algorithm converges at a constant and optimal speed. As shown in Fig. 2, section (x_1, x_2) and the potential section (x_1, x_4) or (x_3, x_2) have a relationship between larger fraction and smaller fraction as

$$\frac{a}{b}=\frac{c}{b}=\frac{b+c}{a}=\varphi \tag{2}$$

If we combine Eqs. (1) and (2), φ can be calculated as

$$\varphi=\frac{1+\sqrt{5}}{2}=1.618\ \ 033\ \ 98 \tag{3}$$

which is the golden ratio, as indicated by the name GSS. After one iteration, the section (x_1, x_2) shrinks from (a+b+c) to either (a+b) or (b+c), and

$$a+b=b+c=0.618\left(a+b+c\right) \tag{4}$$

Thus, the convergence rate R of the GSS is

$$R=\varphi^n \tag{5}$$

where n is the number of iterations.

Based on Eq. (5), only 15 iterations are required for the GSS to shrink the search interval to less than 0.1% of its original length. This means that for a digital control system with 0.1% resolution corresponding to a 10-bit analog-to-digital converter (ADC), no more than 15 iterations are required to obtain the best applicable solution, indicating that the GSS method converges quickly with sufficient accuracy. For example, if there are 1 000 points within an interval, the GSS will find the MPP in no more than 15 iterations, while P&O will require an average of 250 to achieve the same. ε is very similar to the step size in the P&O method. In the voltage range of 0-180 V, the step size can be set as 0.1% of the whole range, i.e., 0.18 V. P&O will require 250 iterations on average to find the MPP, and it will continue oscillating around the MPP with 0.18 V step size. With GSS, it will take no more than 15 iterations to find the MPP within 0.18 V range.

In addition to its fast search speed, the GSS has strengths such as noise-resistive capability and tolerance for measurement errors due to the inherent noises and power ripples in switching-mode converters. This is because the GSS does not require any derivative computation that is easily disturbed by fluctuating signals and noises, and it can automatically change the search direction as the interval shrinks.

Fig. 3 illustrates the principle of the GSS-based MPPT algorithm in single-phase grid-connection PV applications, where V, I, and P represent the PV voltage, current, and power, respectively, and n is the number of iterations. The control objective of the GSS algorithm is the PV voltage V, so it is regulated towards the MPPT voltage (V_{MPPT}) under each iteration. When the width of the interval shrinks to a certain value, called the tolerance ε, it is assumed that V_{MPPT} has been found, and the GSS process ends.

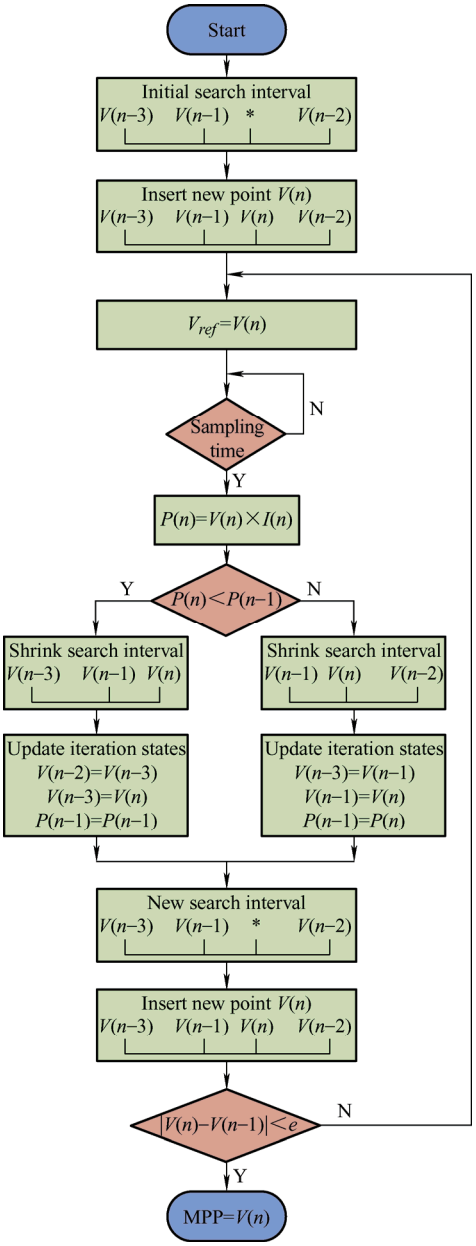

Fig. 3 Principle of GSS-based MPPT algorithm

2.2 GSS-based MPPT with P&O and INC

Besides the GSS process, P&O and INC are integrated into the multi-stage MPPT algorithm for single-phase grid-connected PV systems. The MPPT strategy consists of three stages, each regulated by one of the methods.

In the first stage, P&O with relatively large perturbation steps is used to achieve a fast search speed with the compromise of accuracy. Once V_{MPPT} is located in a narrower range with the relatively simple P&O method, the MPPT enters the second stage, which uses GSS, where the width of the range will be further narrowed at the rate of the golden section ratio. Finally, when the interval width reaches the tolerance value, INC is used to verify the MPP. If the obtained MPP does not drift, the system will operate at the MPP steadily; otherwise, the system must revert back to the first stage.

The detailed procedure is as follows.

(1) P&O: The perturbation steps are counted by number n = 0, 1, 2, ⋯. Starting with n = 0, the initial PV power P_0, and the initial PV voltage V_0, the P&O search steps are as follows.

① Perturb the system with an increment ΔV to V_0, i.e., $V_1=V_0+\Delta V$. ΔV can be positive or negative.

② Observe the output power P_1 under steady state at the new operating point after a time step.

③ Determine whether $P_1>P_0$. If so, maintain the sign of ΔV; otherwise, change the sign of ΔV and swap points 0 and 1 to reestablish $P_1>P_0$. Repeat Step ① and update $V_n=V_{n-1}+\Delta V$.

④ Observe P_n. If $P_n>P_{n-1}$, repeat P&O by adding 1 to n. P&O continues as long as $P_n>P_{n-1}$. Therefore, the power values exhibit an increasing order with $P_n>P_{n-1}>P_{n-2}>\cdots>P_0$.

Once $P_n<P_{n-1}$, the P&O process ends, and the MPP is located within the section (V_{n-2}, V_n). If P&O continues to look for the MPP, the system will oscillate around the MPP with large time step and low accuracy. Therefore, the GSS must start as the next stage.

(2) GSS: With the GSS, the starting interval is now updated as (V_{n-3}, V_{n-2}). The GSS procedure is as follows.

① Insert a point V_{n-1} that divides section (V_{n-3}, V_{n-2}) into two parts that meet the golden section ratio, and (V_{n-3}, V_{n-1}) has a width that is 0.618× that of (V_{n-1}, V_{n-2}).

② Insert another point V_n that divides section (V_{n-3}, V_{n-2}) into two parts that meet the golden section ratio, and (V_{n-3}, V_n) has a width that is 1.618× that of (V_n, V_{n-2}).

③ Compare the power values at V_{n-1} and V_n. If $P_n>P_{n-1}$, the search interval will be shrunk towards the right-hand side, where the point V_{n-2} remains the same, the initial point of V_{n-3} will be updated by the value of V_{n-1}, and the initial point of V_{n-1} will be updated by the value of V_n. If $P_n<P_{n-1}$, the search interval will be shrunk towards the left-hand side, where the point V_{n-1} remains the same, the initial point of V_{n-3} will be updated by the value of V_n, and the initial point of V_{n-2} will be updated by the value of V_{n-3} to ensure that (V_{n-3}, V_{n-1}) has a width that is 0.618× that of (V_{n-1}, V_{n-2}).

④ Insert a new point V_n and repeat Steps ② and ③.

⑤ Once the difference between V_n and V_{n-1} reaches the tolerance value, the MPP is assumed to be found.

(3) INC: An MPP has the mathematical characteristic that $\mathrm{d}P/\mathrm{d}V=0$. In Stage (3), INC aims to validate the MPP obtained in Stage (2) and detect the drift of the MPP under varying weather conditions. The INC procedure is as follows.

① Calculate the slope at the MPP by applying a voltage increment greater than $\mathrm{d}V_{\min}$ to minimize the effect of equipment noise and sampling tolerance.

② Obtain the power increment $\mathrm{d}P$ and calculate the slope $\mathrm{d}P/\mathrm{d}V$.

③ Determine if the absolute value $|\mathrm{d}P/\mathrm{d}V|$ is approximately equal to zero. Assume a small positive tolerance value ε; if $|\mathrm{d}P/\mathrm{d}V|>\varepsilon$, then the MPP obtained in Stage (2) is not correct or has drifted, and the MPPT must start over from Stage (1). Otherwise, $|\mathrm{d}P/\mathrm{d}V|$ can be regarded as approximately equal to zero, and the MPPT has been verified.

Whenever it recognizes the MPP as not correct or having drifted, the GSS-based multi-stage MPPT procedure will restart, and the three stages will be repeated. The full procedure of the multi-stage MPPT strategy is illustrated in Fig. 4.

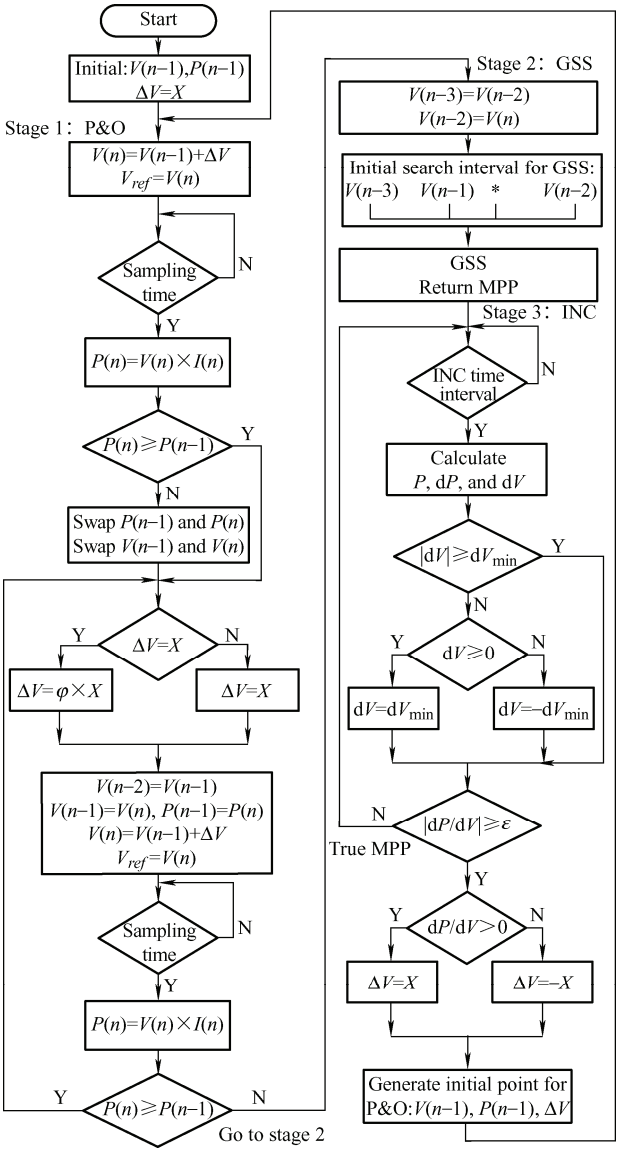

Fig. 4 Procedure of the GSS-based MPPT with P&O and INC

3 System configuration and modeling

The single-phase grid-connected inverter system contains a boost chopper and a dc-ac inverter, where the boost chopper operates in the voltage control mode. The GSS-based multi-stage MPPT strategy is applied to the boost chopper stage, where the output voltage of the PV array is controlled by a proportional-integral (PI) controller to trace the reference generated by the MPPT controller. Both the PI and MPPT controllers are included in the MPPT algorithm block of Fig. 5. While the boost chopper is responsible for tracking the MPP, the inverter is then used to control the dc-link voltage, which indirectly transfers the MPPT power from boost chopper to the grid. When there is a cloud over the PV array, the power extracted by the boost

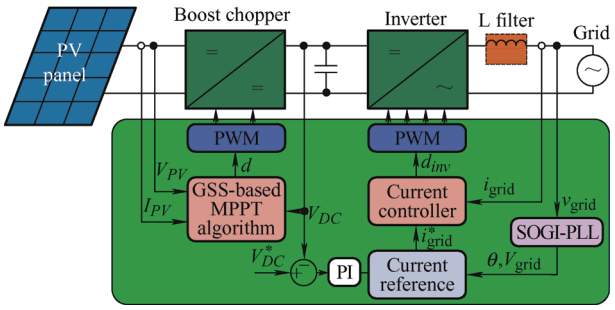

Fig. 5 Control block diagram of the single-phase grid-connected PV system

chopper decreases, while the dc-ac inverter continues to inject the same amount of power into the grid. Thus, the dc-link capacitor must discharge, and the dc-link voltage will decrease. To maintain the dc-link voltage, the dc-ac inverter must reduce the power injected into the grid until it reaches the new MPPT power.

The switching frequency of the boost chopper and the bridge inverter can be different. From the control perspective, it means the front end and following stages are decoupled through the dc-link capacitor. The decoupling control strategy is also suited to multi-input hybrid systems [29], where several input PV modules or wind sources share a common dc bus and inverter.

Fig. 5 shows a control block diagram of the PV system with the GSS-based MPPT algorithm. The PV array block represents the model of the PV characteristics. The voltage controller of the boost chopper and the voltage controller of the inverter are both PI compensators. The reference of the voltage controller for the chopper is given by the MPPT controller. However, the reference voltage of the voltage controller for the inverter is set based on the amplitude of the grid voltage. The predictive control algorithm is employed here in the current controller for the inverter to achieve high-quality grid current injection.

The installed roof PV array consists of 12 modules in total and 3 strings in parallel, where each string has 4 modules in series. The parameters of each module and the whole array are listed in Tab. 1 under normal conditions of 1 000 W/m^2 and 25 ℃. All modules are assumed as identical with the same solar insolation.

Tab. 1 Parameters of PV modules and array

Quantity	Module	Array
Open circuit voltage V_{OC}/V	43.2	172.8
Short circuit current I_{SC}/A	4.7	14.1
Maximum power voltage V_{MPP}/V	34.6	138.4
Maximum power current I_{MPP}/A	4.35	13.05
Maximum power P_{MPP}/W	150	1 800

Mathematical model of the PV array is given by the equation as

$$I=I_{ph}-I_D=I_{ph}-I_o\left(\exp(\frac{q(V_a+IR)}{\pi kT_a})-1\right) \quad (6)$$

where I_{ph} is photocurrent, I_o is saturation current of the diode, q is elementary charge (1.602 176 46×10^{-19} C), n is the diode ideality factor, k is Boltzmann constant (1.380 650 3×10^{-23} J/K), and T_a is absolute temperature.

Following the *I-V* characteristic equation of the PV array from Eq. (6), the nonlinear relationship can be represented by Eq. (7). The values and parameters are all given by the handbook and manual of the manufacturers.

The output current is represented by

$$I=f(V, S, T) \quad (7)$$

where I and V are the output current and output voltage of the PV array, respectively, S is the solar irradiance level, and T is the temperature.

With this equation, the model can be used in the simulation to emulate the practical PV array. Fig. 6 shows both the fitted and the manufacturer's *I-V* and *P-V* characteristics. Fig. 7 shows both the simulated and measured *P-V* curves under various conditions. It shows the fitted characteristic curves match the manufacturer's handbook and measured characteristic curves, which validates the effectiveness of the simulated model.

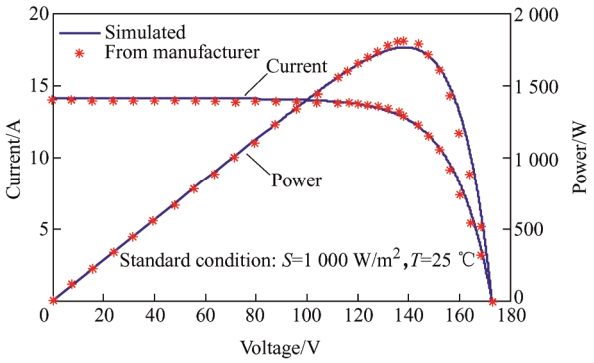

Fig. 6 *I-V* and *P-V* characteristics of PV system with given temperature and insolation

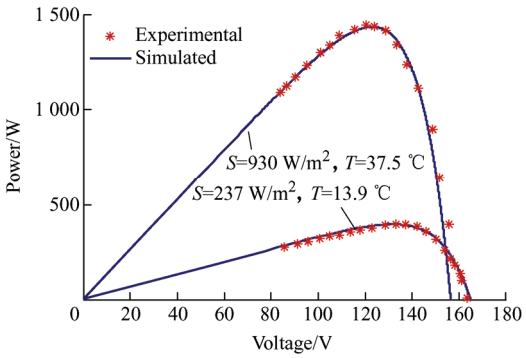

Fig. 7 *P-V* characteristics of the PV array under different conditions

The function of the characteristic curves in Eq. (7) is embedded in the Matlab/Simulink model in Fig. 8. With the given solar insolation and temperature, the characteristic curves can determine the relationship between the voltage V and current I at the PV terminal. With a specific load, there exists a unique operating equilibrium point, which can be automatically obtained then this block is inserted model into the Matlab/Simulink model.

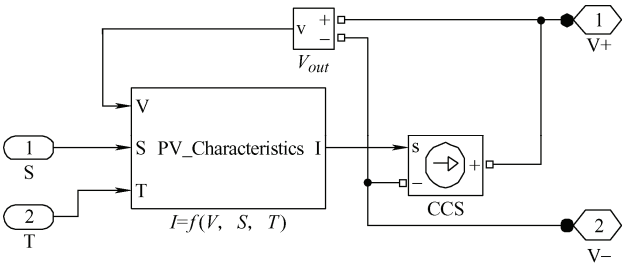

Fig. 8 Simulink model for PV array

To verify the GSS-based multi-stage MPPT algorithm, the system shown in Fig. 9 was built in Matlab/Simulink. The PV array as described by Fig. 8 is represented by the block "PV Array" in Fig. 9, and the GSS-based multi-stage MPPT algorithm is implemented as an S-function module written in C language. The system parameters in simulation are configured to match the real system. For simplicity, a 200 V battery is connected as the load of the boost chopper in the simulation for the MPPT performance.

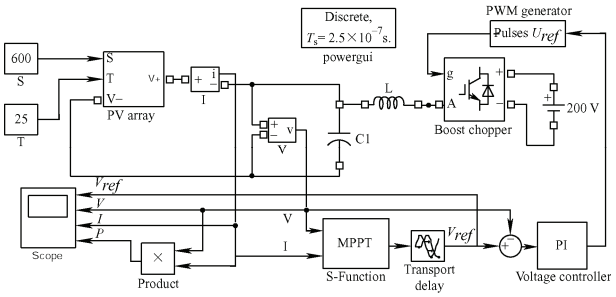

Fig. 9 Simulink diagram for the single-phase grid-connected inverter system

4 Simulation and experimental results

4.1 Simulation results

The simulation of the proposed MPPT technique was run in Matlab/Simulink with the ode23t solver and sampling step size 1×10^{-7}. Figs. 10 and 11 show the simulation results of the proposed multi-stage MPPT and P&O/INC under different solar insolation and temperatures, which include the boost chopper voltage reference V_{ref}, PV terminal voltage V, current I, and output power P. The time interval of the search step is set as 3 ms. The search step should be greater than the settling time to ensure that the system is able to track the updated MPPT during each time interval.

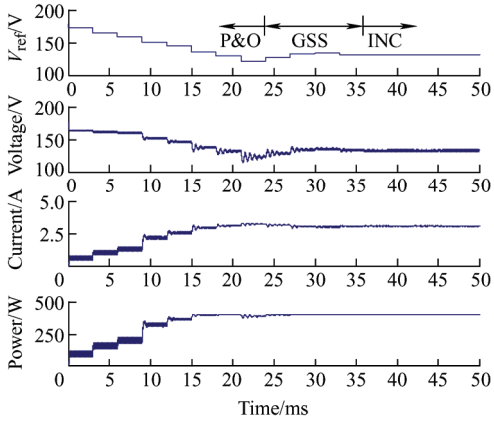

(a) GSS-based multi-stage MPPT

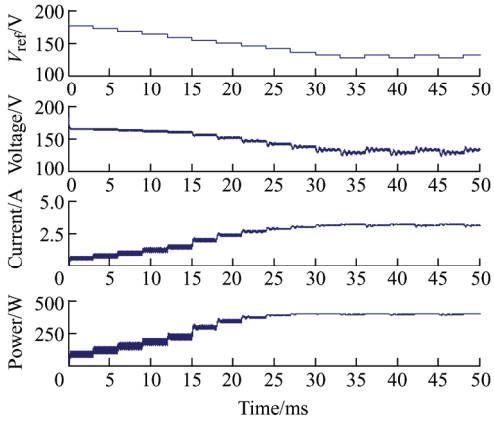

(b) P&O/INC

Fig. 10 Simulation results under the conditions of S=237 W/m^2, T=13.9 ℃

From Fig. 10a, the GSS-based multi-stage MPPT has 3 stages. Firstly, P&O stage of the proposed MPPT technique has 8 search steps to successfully locate the vicinity area. Secondly, GSS stage takes another 4 search steps to reach the MPP. Therefore, with 3 ms for each time interval, the search time in total is 36 ms. Finally, INC stage verifies the located MPP, and the system reaches steady state. The steady-state output power under steady state is 397.7 W compared with the maximum PV output power of 397.9 W. The MPPT efficiency is as high as 99.95%. In contrast, the simulation results for the system with P&O/INC are shown in Fig. 10b. The perturbation step size was chosen optimally as 4.5 V for P&O/INC to achieve almost the same search speed as the proposed multi-stage MPPT technique. In this manner, there exists oscillation under steady state, the average output power is reduced to 395.3 W, and the MPPT efficiency is reduced to 99.35%.

Under a different solar insulation and temperature of S=930 W/m^2, T=37.5 ℃, Fig. 11 shows the similar results. From Fig. 11a, firstly, P&O stage of the proposed MPPT technique has 7 search steps to successfully locate the vicinity area. Secondly, GSS stage takes another 5 search steps to reach the MPP. Therefore, with 3 ms for each time interval, the search time in total is 36 ms. Finally, INC stage verifies the located MPP, and the system reaches steady state. The steady-state output power and search accuracy are 1 438.6 W and 99.94%, respectively, as been put in Tab. 2. In contrast, the simulation results for the system with P&O/INC are shown in Fig. 11b. The search time of P&O/INC is close to 36 ms, but the output power drops to 1 437.3 W and the MPPT efficiency becomes 99.85%.

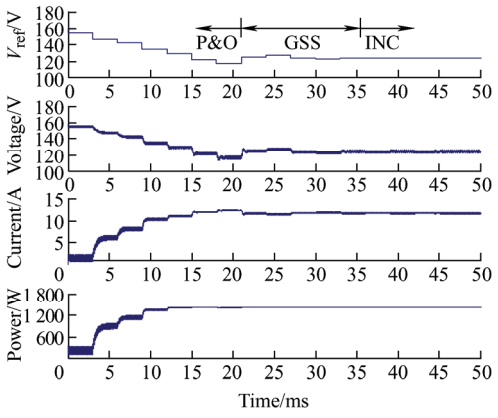

(a) GSS-based multi-stage MPPT

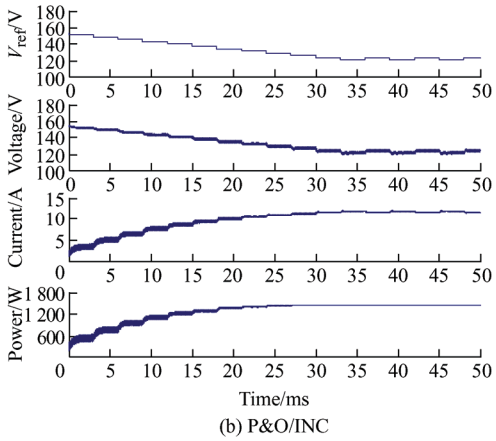

(b) P&O/INC

Fig. 11 Simulation results under the conditions of S=930 W/m^2, T=37.5 ℃

Tab. 2 Search time and accuracy results for different MPPT methods

MPPT methods	Search time/ ms	Search accuracy (%)
Proposed multi-stage MPPT with GSS	36	99.94
P&O [9]	28 500	98.28
Modified adaptive hill climbing [9]	23 500	98.45
Fixed step size INC [14]	7 500	98.90
Variable step size INC [14]	1 500	99.20

Some facts should be noted from the simulation results, for example, the ripples of the voltage are the most prominent because the search continues even after MPP has been found. In other words, the MPPT algorithm still perturbs the located voltage to verify if the located MPP is the real MPP. According to the P-V characteristic shown in Fig. 7, around the MPP, the voltage oscillation does not necessarily lead to power oscillation.

4.2 Experimental results

In addition to the simulations, verification experiments were conducted on the real system. The experimental setup was based on a wind/solar hybrid inverter system, where the wind has a power rating of 10 kW and the PV has a power rating of 2 kW. The wind power system is paralleled with the PV system at the dc-link through a diode rectifier and boost converter. The experimental setup is shown in Fig. 12, where a DSP TMS320F28335 was used as the microcontroller to implement the GSS-based MPPT algorithm. The following figures show the data obtained from the experiment and plotted in Matlab.

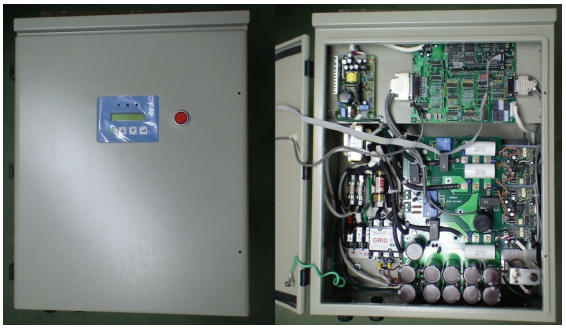

Fig. 12 Prototype of hybrid PV and wind converter

Fig. 13 plots the GSS-based multi-stage MPPT performance under certain weather conditions. The experimental results are consistent with the simulation results in Figs. 10 and 11 for the same weather conditions. Fig. 14 shows the system behavior under minor environmental condition changes. The real system can catch up with condition changes within 30 ms, which is also consistent with the simulation results.

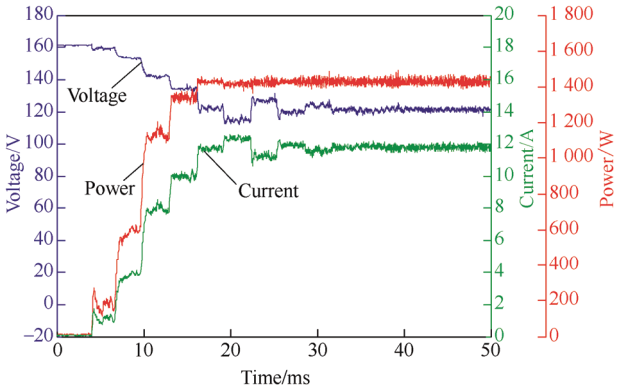

Fig. 13 Experimental waveforms of GSS-based MPPT with insolation of 930 W/m^2 and temperature of 37.5 ℃

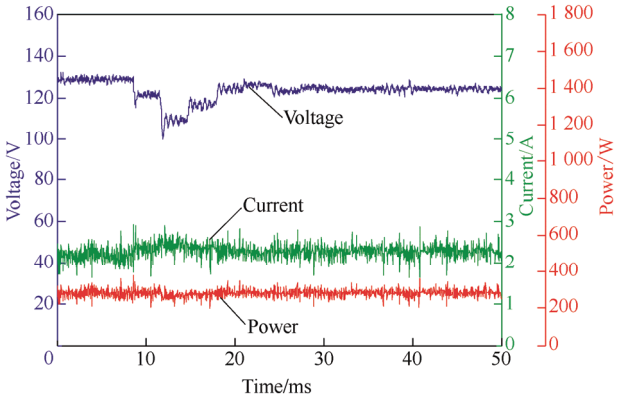

Fig. 14 Transient response of the GSS-based MPPT algorithm with disturbance of solar insolation

Fig. 15 plots the steady state waveforms of the grid voltage, current, and dc-link voltage. The grid current must be in phase with the grid voltage for a unity power factor. The dc-link voltage was set to 200 V. As discussed previously, 120 Hz ripples exist in the dc-link voltage. However, the ripples barely affect the quality of the output current of the inverter. In this case, the total harmonic distortion (THD) of the current is 1.8%, and the power factor is unity. The search time and accuracy of the proposed multi-stage MPPT method with GSS are compared with other MPPT methods in Tab. 2, where the proposed MPPT method improves the search time significantly compared with P&O and INC under grid-connected operation. The search times of P&O and INC are highly dependent on the step sizes of the corresponding methods. The search time of P&O and INC can be significantly improved by sacrificing search accuracy.

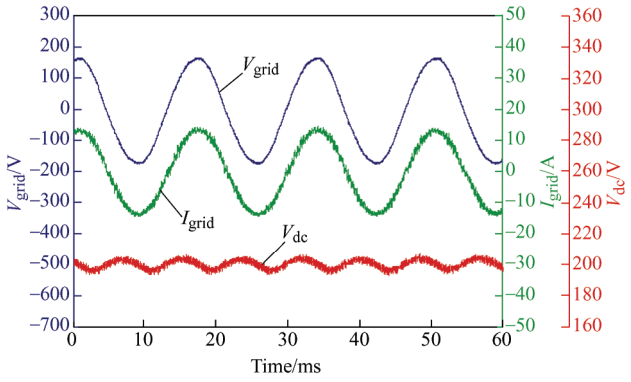

Fig. 15 Experimental waveforms of the single-phase grid-connected inverter

5 Conclusions

In this paper, a GSS-based multi-stage MPPT technique that combines GSS with P&O and INC was proposed to achieve fast convergence to the MPP with small oscillation. The proposed multi-stage MPPT technique starts by searching the vicinity of the MPP by P&O in the first stage. Then, it quickly narrows the width of the interval with the golden ratio in the second stage, and the located MPP by is verified by the INC method in the third stage. The advantages of P&O, GSS, and INC are exploited, while their disadvantages are avoided. Therefore, this MPPT algorithm provides fast response and high tracking efficiency, as shown through the simulation and experimental results. The simulation and experimental results verified the feasibility and effectiveness of the proposed MPPT technique.

The proposed MPPT technique mainly targets the MPP of a unimodal function, i.e., the curve has only one extremum, but it is not suited to multimodal functions, i.e., the curve has multiple extrema when partial shading happens. Thus, to apply the proposed MPPT technique to partial shading conditions, more points must be inserted into the GSS scheme to locate the MPP. The application of the proposed MPPT technique under the partial shading condition remains as future work.

References

[1] U.S. Energy Information Administration (EIA), Where solar is found and used. [2020-09-05]. https://www.eia.gov/energyexplained/solar/where-solar-is-found.php.

[2] L Zhang, F K Jiang, D W Xu, et al. Two-stage transformerless dual-buck PV grid-connected inverters with high efficiency. *Chinese Journal of Electrical Engineering*, 2018, 4(2): 36-42.

[3] S Xu, L Chang, R Shao. Evolution of single-phase power converter topologies underlining power decoupling. *Chinese Journal of Electrical Engineering*, 2016, 2(1): 24-39.

[4] R W Erickson, D Maksimovic. Fundamentals of power electronics. Boston: Springer, 2001.

[5] P K Bonthagorla, S Mikkili. Performance investigation of hybrid and conventional PV array configurations for grid-connected/standalone PV systems. *CSEE J. Power Energy Syst.*, 2020: 1-16.

[6] C Schaef, J T Stauth. Multilevel power point tracking for partial power processing photovoltaic converters. *IEEE J. Emerg. Sel. Top. Power Electron.*, 2014, 2(4): 859-869.

[7] F Li, C B Li, K Sun, et al. Capacity configuration of hybrid CSP/PV plant for economical application of solar energy. *Chinese Journal of Electrical Engineering*, 2020, 6(2): 19-29.

[8] N Femia, G Petrone, G Spagnuolo, et al. Optimization of perturb and observe maximum power point tracking method. *IEEE Trans. Power Electron.*, 2005, 20(4): 963-973.

[9] W D Xiao, W G Dunford. A modified adaptive hill climbing MPPT method for photovoltaic power systems. *in 2004 IEEE 35th Annual Power Electronics Specialists Conference (IEEE Cat. No.04CH37551)*, 2004, 3(3):

1957-1963.

[10] M Dehghani, M Taghipour, G B Gharehpetian, et al. Optimized fuzzy controller for MPPT of grid-connected PV systems in rapidly changing atmospheric conditions. *J. Mod. Power Syst. Clean Energy*), 2020: 1-8.

[11] A Safari, S Mekhilef. Simulation and hardware implementation of incremental conductance MPPT with direct control method using Cuk converter. *IEEE Trans. Ind. Electron.*, 2011, 58(4): 1154-1161.

[12] E Roman, R Alonso, P Ibanez, et al. Intelligent PV module for grid-connected PV systems. *IEEE Trans. Ind. Electron.*, 2006, 53(4): 1066-1073.

[13] A Pandey, N Dasgupta, A K Mukerjee. Design issues in implementing MPPT for improved tracking and dynamic performance. *in IECON 2006 - 32nd Annual Conference on IEEE Industrial Electronics*, 2006: 4387-4391.

[14] F Liu, S Duan, F Liu, et al. A variable step size INC MPPT method for PV systems. *IEEE Trans. Ind. Electron.*, 2008, 55(7): 2622-2628.

[15] N Femia, G Petrone, G Spagnuolo, et al. A technique for improving P&O MPPT performances of double-stage grid-connected photovoltaic systems. *IEEE Trans. Ind. Electron.*, 2009, 56(11): 4473-4482.

[16] H Rezk, M Aly, M Al-Dhaifallah, et al. Design and hardware implementation of new adaptive fuzzy logic-based MPPT control method for photovoltaic applications. *IEEE Access*, 2019(7): 106427-106438.

[17] F Lin, K Lu, B Yang. Recurrent fuzzy cerebellar model articulation neural network based power control of a single-stage three-phase grid-connected photovoltaic system during grid faults. *IEEE Transactions on Industrial Electronics*, 2017, 64(2): 1258-1268.

[18] F Fateh, W N White, D Gruenbacher. A maximum power tracking technique for grid-connected DFIG-based wind turbines. *IEEE J. Emerg. Sel. Top. Power Electron.*, 2015, 3(4): 957-966.

[19] R C N Pilawa-Podgurski, W Li, I Celanovic, et al. Integrated CMOS energy harvesting converter with digital maximum power point tracking for a portable thermophotovoltaic power generator. *IEEE J. Emerg. Sel. Top. Power Electron.*, 2015, 3(4): 1021-1035.

[20] B Subudhi, R Pradhan. A comparative study on maximum power point tracking techniques for photovoltaic power systems. *IEEE Trans. Sustain. Energy*, 2013, 4(1): 89-98.

[21] T Esram, P L Chapman. Comparison of photovoltaic array maximum power point tracking techniques. *IEEE Trans. Energy Convers.*, 2007, 22(2): 439-449.

[22] N C Swanepoel, C G Richards, A F Nnachi, et al. A comparative study of maximum power point tracking algorithms for PV arrays. *in 2020 6th IEEE International Energy Conference (ENERGYCon)*, 2020: 819-823.

[23] B Mbarki, F Farhani, A Zaafouri. Comparative study of some maximum power point tracking algorithms. *in 2019 International Conference on Signal, Control and Communication (SCC)*, 2019: 145-149.

[24] A Ibrahim, MB Shafik, Min Ding, et al. PV maximum power-point tracking using modified particle swarm optimization under partial shading conditions. *Chinese Journal of Electrical Engineering*, 2020, 6(4): 106-121.

[25] Z Yi, Y Xu, W Gu, et al. Distributed model predictive control based secondary frequency regulation for a microgrid with massive distributed resources. *IEEE Transactions on Sustainable Energy*, 2021, 12(2): 1078-1089.

[26] E I Batzelis, S A Papathanassiou, B C Pal. PV system control to provide active power reserves under partial shading conditions. *IEEE Transactions on Power Electronics*, 2018, 33(11): 9163-9175.

[27] P E Gill, W Murray, M H Wright. Practical optimization. Pittsburgh: Academic Press, 1981.

[28] R M Shao, L C Chang. A new maximum power point tracking method for photovoltaic arrays using golden section search algorithm. *in 2008 Canadian Conference on Electrical and Computer Engineering*, 2008: 000619-000622.

[29] Y Chen, Y Liu, S Hung, et al. Multi-input inverter for grid-connected hybrid PV/wind power system. *IEEE Trans. Power Electron.*, 2007, 22(3): 1070-1077.

Shuang Xu (S'15-M'18) received the B.Sc.E.E. in 2012 from Hefei University of Technology, Hefei, China, and the Ph. D. in Electrical Engineering in 2018 at the University of New Brunswick (UNB), Fredericton, Canada.

He was a Post-Doctoral Fellow with the Emera and NB Power Research Centre for Smart Grid Technologies at UNB and a Post-Doctoral Associate at Western University, London, Canada, from 2018 to 2021. He is currently a Guest Professor in the School of Electrical and Control Engineering at North China University of Technology, Beijing, China. His research interests include renewable energy systems, energy storage technologies, power electronics, and power system support functions for distributed energy resources.

Dr. Xu was a recipient of the IEEE Applied Power Electronics Conference Outstanding Presentation Award in 2017. He was the Tutorial Speaker in IEEE PEDG 2019, 2021, IEEE CPERE 2019, IEEE HVDC 2020, and Session Chair of the IEEE Symposium on Power Electronics for Distributed Generation Systems (PEDG 2019). He also serves as the Treasurer in 2018 and the Chair in 2019 of IEEE UNB Power Electronics Society Student Branch Chapter.

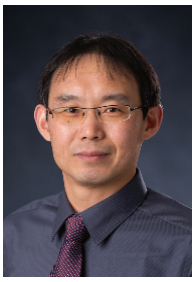

Riming Shao (M'08) received the B.Sc.E.E. in 1994 and M.Sc. in 1997 from Tongji University, Shanghai, China; and the Ph.D. degree in 2010 from the University of New Brunswick, Fredericton, Canada. He currently works as a Project Engineer with Alpha Technologies at Bellingham, Washington State, USA. His research interests include smart grids, power converters, renewable energy systems, and distributed power generation systems.

Dr. Shao is a registered Professional Engineer of Engineers and Geoscientists New Brunswick, Canada.

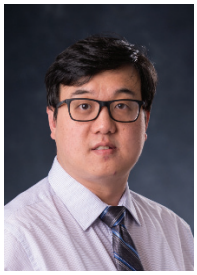

Bo Cao (S'08-M'15) received the B.Sc.E. degree from East China University of Science and Technology, Shanghai, China, in 2005; and the Ph.D. degree from the University of New Brunswick, Fredericton, NB, Canada, in 2015. He is currently a Research Associate with the Emera and NB Power Research Centre for Smart Grid Technologies at the University of New Brunswick. His principle research interests include power converter design, grid-integration technology, distributed generation system and smart grid techniques.

Liuchen Chang (S'80-M'92-SM'99) received B.S.E.E. from Northern Jiaotong University in 1982, M.Sc. from China Academy of Railway Sciences in 1984, and Ph.D. from Queen's University in 1991. He joined the University of New Brunswick in 1992 and is a Professor in Electrical and Computer Engineering. He was the NSERC Chair in Environmental Design Engineering during 2001-2007, and was the Principal Investigator of Canadian Wind Energy Strategic Network (WESNet) during 2008-2014. He is currently the President of the IEEE Power Electronics Society.

Dr. Chang was a recipient of CanWEA R.J. Templin Award in 2010 for his contribution in the development of wind energy technologies, and the Innovation Award for Excellence in Applied Research in New Brunswick in 2016. He is a Fellow of Canadian Academy of Engineering (FCAE). He has published more than 340 refereed papers in journals and conference proceedings. Dr. Chang has focused on research, development, demonstration and deployment of renewable energy based distributed generation systems and direct load control systems.